Mon. Not. R. Astron. Soc. **000**, 000–000 (0000) Printed 1 February 2008 (MN LATEX style file v2.2)

Dark halo properties from rotation curves

Raul Jimenez[1], Licia Verde[1,2] and S. Peng Oh[3]
[1] *Department of Physics and Astronomy, Rutgers University, 136 Frelinghuysen Road, Piscataway, NJ 08854–8019, USA.*
[2] *Princeton University Observatory, Princeton, NJ 08544, USA.*
[3] *Theoretical Astrophysics, Mail Code 130-33, Caltech, Pasadena, CA 91125, USA.*

1 February 2008

ABSTRACT
We study a large set of high spatial resolution optical rotation curves of galaxies with the goal of determining the model parameters for a disk embedded within a cold dark matter (CDM) halo that we model either with a Navarro, Frenk & White (NFW) profile or pseudo-isothermal profile. We show that parameter degeneracies present in lower resolution data are lifted at these higher resolutions. 34% of the galaxies do not have a meaningful fit when using the NFW profile and 32% when using the pseudoisothermal profile, however only 14% do not have a meaningful fit in either model. In both models we find correlations between the disk baryon fraction f_d and the spin parameter of the halo λ', between f_d and the dark halo mass M_{200}, and between M_{200} and the concentration parameter c. We show that the distribution of the concentration parameters c, for a NFW halo, is in good agreement with CDM predictions; no significant galaxy population is found with very low values of c. The overall distribution of λ' is in good agreement with theoretical predictions from hierarchical tidal torque theory. The whole sample is also well fitted by a pseudo-isothermal dark halo with a core, but the size of the core is rather small (6% of the virial radius or smaller; for 70% of the sample the core size is less than 2 kpc). Thus we conclude that the profile of dark matter is steep (r^{-1} or steeper) down to this radius; large dark matter cores (and therefore very low dark matter central densities) seem to be excluded. LSBs tend to have higher values of λ' for a given f_d and lower values of c for a given mass than HSBs. In an appendix we give some useful formula for pseudo-isothermal profile halos and discuss in detail the issue of parameter degeneracies.

Key words: cosmology: theory — galaxies: formation — galaxies: spiral — galaxies: kinematics and dynamics

1 INTRODUCTION

The Cold Dark Matter (CDM) paradigm for structure formation has proved remarkably successful in explaining the observed large-scale properties of the universe, such as the abundance and clustering of galaxies and clusters (Peacock et al 2001; Verde et al. 2001; Lahav et al. 2001), the statistical properties of the Lyα forest (e.g., Phillips et al. (2001)), and the power spectrum of the cosmic microwave background anisotropies (e.g., Jaffe et al (2001)). However, a number of puzzling discrepancies remain when CDM predictions are extrapolated to small scales. Chief among them are: (i) The substructure problem. CDM over-predicts the number of satellites around a Milky-Way sized galaxy by an order of magnitude (Klypin et al. 1999; Moore et al. 1999). (ii) The density profile problem. Observed rotation-curves of dwarf and lower surface brightness galaxies suggest that the inner regions have a constant density core rather than the density cusp predicted by CDM (e.g., McGaugh & de Blok (1998); Moore et al. (1999); Dalcanton & Bernstein (2000)).

Furthermore, numerical SPH simulations of disk formation within dark halos fail to match the zero-point of the observed Tully-Fisher. One possible solution is to lower the central concentration of the dark matter halos (Navarro & Steinmetz 2000b).

These problems have stimulated numerous proposed astrophysical solutions, as well as modifications of the fundamental CDM paradigm itself (e.g., Spergel & Steinhardt (2000); Kamionkowski & Liddle (2000); Colombi, Dodelson & Widrow (1996); Bode, Ostriker & Turok (2001); Goodman (2000); Hu, Barkana & Gruzinov (2000); Cen (2001)).

In this paper we once again examine the density profile problem by fitting CDM models to observed rotation curves of spiral galaxies. Our study differs from previous work in two respects. Firstly, we use optical rotation curves rather than the HI rotation curves used in previous studies which are plagued by beam smearing (Swaters et al. 2000; van den

Bosch et al. 2000). Even if the effects of beam smearing are neglected, the relatively large errors and limited spatial sampling of HI rotation curves imply that they cannot be used to discriminate between constant density cores and r^{-1} cusps (van den Bosch & Swaters 2001). By contrast, the optical rotation curves we use are free from beam smearing, have smaller errors and higher spatial resolution. We show that, with this superior data, various parameter degeneracies present when fitting HI rotation curves can be lifted. This allows us to distinguish between core and cusp-like inner profiles. Secondly, while many studies have focused on relatively small samples of dwarfs (but see Navarro (1998)), we use a large sample (400 galaxies) spanning a wide range in luminosity and surface brightness.

Our goal is to determine the best fitting model parameters for a disk within the CDM profile proposed by Navarro Frenk and White (1997; NFW) and within a pseudo-isothermal profile halo and study the distributions of the recovered disk parameters.

We find that the NFW profile provides a good fit to 66% of the galaxies in the sample, with a distribution of recovered concentration parameters and spin parameters broadly consistent with that predicted by CDM numerical simulations. When the sample is fitted with an isothermal profile with a core, 68% of the galaxies are well fitted whithin this model and the best fit parameters favor cores with small sizes (below 6% of the dark halo virial radius). Many rotation curves that have no meaningful fit in one dark matter profile are well fitted by the other. There is no meaningful fit in either model for only for 14% of the sample. This is consistent with the inner dark matter profiles being steep (slope of -1 or steeper) down to radii that are few percent of the virial radius.

In both models the recovered baryonic mass to light ratios are broadly in agreement with predictions from synthetic stellar populations.

This paper is organized as follows. In section 2 we present the set of rotation curves we analyze and the two models we use to fit the data (exponential disk embedded in a dark matter halo with a NFW profile or a pseudo-isothermal profile). These two models have four free parameters, but since for most of the galaxies the scale length of the disk is given, we report the analysis for four free parameters in appendix II and present in the main text the results for the fit with three free parameters. In section 3 we illustrate and discuss the correlations we find between the best fit parameters for the two models. We discuss the general implications of these findings in section 4 where we also compare the derived baryonic mass-to-light ratios with the range allowed by stellar populations. Finally, we conclude and summarize our results in section 5. In appendix I we develop the expression for the rotation curve of an exponential disk embedded in a pseudoisothermal halo. In appendix III we study the degeneracies among the parameters of the models.

2 ROTATION CURVES

We study a large set of observed rotation curves of galaxies with the aim of determining the model parameters for a disk within a NFW (Navarro, Frenk & White 1997) profile halo and within a pseudo-isothermal profile halo (i.e., an isothermal sphere with a constant density core). The choice of a pseudo-isothermal halo is motivated by recent claims in the literature that the dark matter profile of low–surface brightness galaxies (LSB, e.g., de Blok et al. (2001)) and some high–surface brightness galaxies (HSB, e.g., Salucci (2001); Borriello & Salucci (2001); Salucci & Burkert (2000)) is better represented by a flat core rather than the steeper profile found in CDM N-body simulations.

2.1 The observational sample

We use three sets of observed rotation curves. The first is the catalog compiled by Courteau (1997) (Courteau sample) which consists of optical H_α long–slit rotation curves for 300 Sb–Sc UGC galaxies and R-band photometry. The second is a sample of 74 spiral galaxies (Sa–Sd) observed again in the optical (H_α) by Palunas & Williams (2000) (PW sample). For this sample I–band photometry and the velocity field in two dimensions is available. Finally, we also consider the recently published optical (H_α) rotation curves for 26 Low Surface Brightness (LSB) galaxies by McGaugh, Rubin & de Blok (2001). These consist of long slit H_α observations for 26 galaxies and B-band photometry for a smaller sample. In total we have 400 optical rotation curves.

All three samples provide inclination corrected curves with their corresponding errors. The Courteau and PW samples have surface photometry and give values for the stellar disk scale lengths, but we do not have disk scale lengths for the LSB sample.

The sample of galaxies studied here is somewhat heterogeneous: we use LSB and HSB galaxies; some curves have much smaller error-bars than others, and the sampling range of the rotation curve varies significantly: in particular, some curves do not extend to large enough radii to show the flattening of the rotation curve. The diversity of the sample is both a strength as well as a weakness: it allows us to probe general statistical trends across a wide range of galaxy luminosities and surface brightness.

2.2 The models

Many authors have investigated galactosynthesis models (Dalcanton, Spergel & Summers 1997; Jimenez, Heavens, Hawkins & Padoan 1997; Mo, Mao & White 1998; Jimenez, Padoan, Matteucci & Heavens 1998; Somerville & Primack 1999; van den Bosch 2000; Avila-Reese & Firmani 2000; Firmani & Avila-Reese 2000; Navarro & Steinmetz 2000b) in which the properties of disk galaxies are determined primarily by the mass, size, and angular momenta of the halos in which they form, and which may contain the effects of supernova feedback, adiabatic disk contraction, cooling, merging, and a variety of star-formation recipes. In this paper, we are mainly concerned with the dynamical properties of the disk/halo system which affect the rotation curve, in the spirit of Dalcanton et al. (1997); Jimenez et al. (1997), and Mo, Mao & White (1998) (hereafter MMW). We model spiral galaxies as exponential disks (i.e., disks with surface density profiles $\Sigma(r) = \Sigma_0 \exp(-r/R_d)$, where R_d is the scale length of the disk) embedded within CDM halos which we model either with NFW profiles or pseudo-isothermal

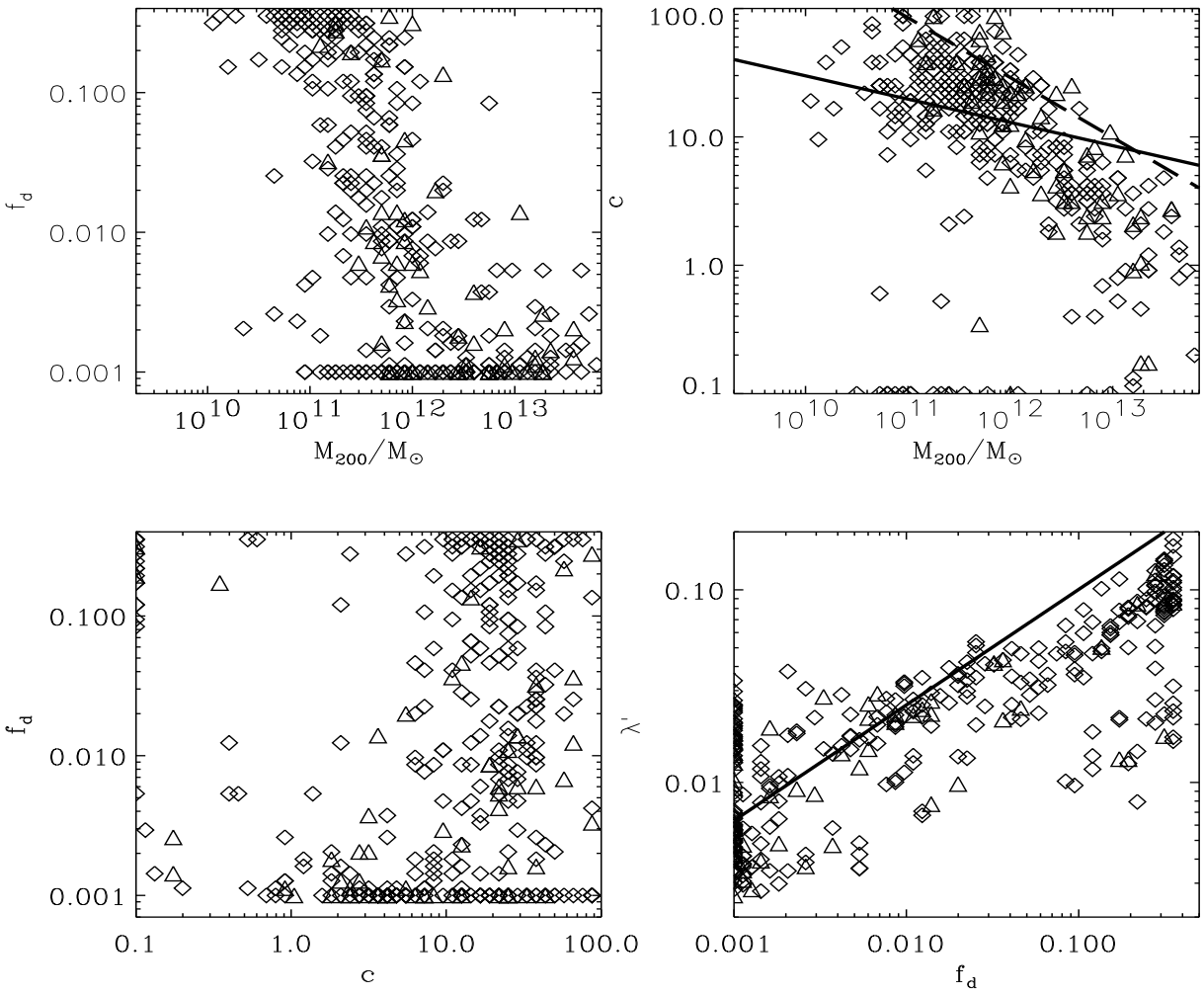

Figure 1. NFW model. The location of the sample of galaxies in different projections of the three dimensional parameter space (M_{200}, f_d, c) when fitted with a NFW dark halo model. The diamonds correspond to galaxies from Courteau (1997) and the triangles are from Palunas & Williams (2000). The solid and dashed lines in the top-right panel are the N-body simulations predictions for the c-M_{200} correlation (see text for more details). Also plotted (bottom-right panel) is the deduced value for λ' vs. f_d. The solid line is the least square fit from 14 dwarfs by Burkert (2000), in good agreement with the correlation found here from 362 galaxies. Note also the correlation between f_d and M_{200}.

spheres. In both models we assume that the baryons initially follow the same density profile as the dark matter and then cool and settle into an exponential disk in a dynamical time. We assume that the baryons that do not settle in the disk follow the dark matter distribution. The disks have a mass fraction $f_d \equiv M_{\rm disk}/M_{200} \leqslant \Omega_b/\Omega_m$. Here $M_{\rm disk}$ denotes the baryonic mass that settle into an exponential disk, M_{200} denotes the mass within a radius R_{200} that encloses an average density 200 times the critical density, Ω_m denotes the density parameter and Ω_b the baryon contribution to the density parameter. Throughout, we assume a ΛCDM cosmology given by: $(\Omega_m, \Omega_\Lambda, \Omega_b, h, \sigma_{8h^{-1}}) = (0.3, 0.7, 0.039, 0.7, 1.0)$.

In these models, the rotation velocity is given by:

$$V_c^2(r) = V_d^2 + V_{\rm CDM}^2 \tag{1}$$

where the baryonic disk rotation velocity is (Binney & Tremaine (1987), p. 77)

$$V_d^2(r) = 4\pi G \Sigma_0 R_d y^2 \left[I_0(y)K_0(y) - I_1(y)K_1(y)\right] , \tag{2}$$

with $y = r/(2R_d)$, $\Sigma_0 = f_d M_{200}/(2\pi R_d^2)$, I_n and K_n denoting the modified Bessel functions of the first and second kind. The contribution to the rotation curve from the dark matter is:

$$V_{\rm CDM}^2(r) = GM_{\rm CDM}(r)/r, \tag{3}$$

where $M(r)$ denotes the mass enclosed within the radius r. For a model to be fully specified, we require expressions for the disk scale length R_d and for $M(r)$.

The NFW fit to the density profile of dark matter found in collisionless N-body numerical simulations is:

$$\rho(r) = \rho_{\rm crit} \frac{\delta_0}{(r/r_c)(1+r/r_c)^2} \tag{4}$$

where $\rho_{\rm crit}$ is the critical density ($\rho_{\rm crit} = 277.3h^2$ $M_\odot$ kpc^{-3}) and r_c is roughly the break radius at which the

slope of the profile changes from -1 to -3. The concentration parameter c is defined as $c = R_{200}/r_c$, where $R_{200} = (M_{200}/(4/3\pi 200\rho_{\rm crit}))^{1/3}$ and M_{200} is assumed to be the total mass of the dark matter halo. The dark matter mass within an enclosed radius r is:

$$M(r) = 4\pi\rho_{\rm crit}\delta_0 r_c^3 \left[\frac{1}{1+cx} - 1 + \ln(1+cx)\right], \quad (5)$$

where $x = r/R_{200}$. From equation (5), the relation between δ_0 and c is:

$$\delta_0 = \frac{200}{3}\frac{c^3}{\ln(1+c) - c/(1+c)}. \quad (6)$$

Disk formation affects the dark matter profile by the adiabatic contraction it induces in the inner regions of the dark matter halo. As in MMW, we model this by assuming that the halo responds adiabatically to the slow contraction of the disk, and therefore that the angular momentum of dark matter particles is conserved. This yields the relation between the initial radius r_i and final radius r where a dark matter particle ends up:

$$GM_f(r)r = GM(r_i)r_i \quad (7)$$

where $M(r_i)$ is given by equation (5), and $M_f(r) = \Sigma_o \exp(-r/R_d) + M(r_i)(1-f_d)$ is the total final mass within r (see MMW for details).

Assuming angular momentum conservation, MMW developed a fitting formula for $R_d(c, M_{200}, \lambda', f_d)$ which we use (see their equations (28) and (32)). Note that we use the modified spin parameter $\lambda' \equiv (j_d/f_d)\lambda$, where $j_d \equiv J_d/J$ and J_d, J are the total angular momentum of the disk and halo respectively. If the specific angular momentum of the disk is equal to that of the halo, then $j_d = f_d$ and $\lambda' = \lambda$.

In the NFW model, for a given M_{200}, the overdensity δ_0 and thus the concentration parameter c depends on the collapse redshift. There is therefore a correlation between c and M_{200}, since more massive halos collapse at lower redshift than less massive ones. However, there is a fairly wide scatter in the distribution of c for fixed M_{200} (e.g., Jing (2000)). Furthermore, there is growing observational evidence that the distribution of concentration parameters might not be as predicted by CDM (e.g., Navarro & Steinmetz (2000b); Keeton (2001)); one of the goals of this paper is to explore this question further. We therefore keep c as a free parameter. Thus, there are four free parameters in our model: the spin of the dark halo λ', the mass of the dark halo M_{200}, the concentration parameter c and the fraction of the total mass in the disk f_d.

For the pseudo-isothermal sphere the profile of the dark matter is:

$$\rho = \rho_0 \left[1 + \left(\frac{r}{r_c}\right)^2\right]^{-1} \quad (8)$$

where ρ_0 denotes the finite central density. We have developed a similar analytic model to compute the properties of an exponential disk in this profile (see Appendix I). In this case, we do not include the adiabatic compression of the halo due to the baryons, since we want to use a constant density inner core for the final dark matter distribution by fiat. In the pseudo-isothermal profile case, the CDM rotation velocity is:

$$V^2_{\rm CDM} = 4\pi G\rho_0 r_c^2 \left[1 - \frac{r_c}{r}\arctan\left(\frac{r}{r_c}\right)\right]. \quad (9)$$

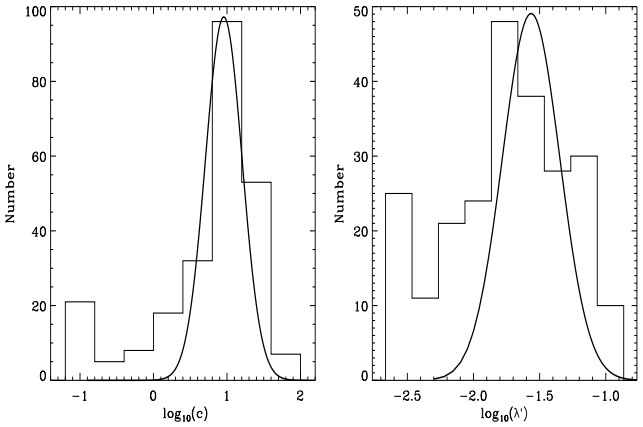

Figure 2. NFW model. The distribution of c (left panel) and λ' (right panel) deduced from NFW halos fits to rotation curves. Also over-plotted as continuous lines are the theoretical predictions for each of these parameters. Note that the derived values of c are broadly in agreement with the predictions from N-body simulations (see text for more details).

A fitting formula for the disk scale length R_d as a function of M_{200}, c, f_d and λ' for this profile is given in Appendix I. Any rotation curve can be fitted with this profile using four parameters: λ', M_{200}, r_c, f_d.

For each galaxy rotation curve we explore the whole likelihood surface and the best fitting model is then obtained using a standard χ^2 minimization.

We discuss in detail the values for the disk parameters found for these two models (NFW and pseudoisothermal) when using all four free parameters in Appendixes II and III. In this section we eliminate one of the four free parameters (λ') by using the observed scale lengths of the exponential disks R_d. Then the only remaining free parameter for the baryonic disk is f_d. Since we do not have R_d for the LSB sample and for some of the galaxies in the PW sample, the analysis with three free parameters is performed on the Courteau and PW samples (in total 362 galaxies). The disk parameter distributions for the four parameters fit is quite similar to that for the three parameter fit. We discuss the locus of LSB galaxies in the parameter space in Appendix II and show that they follow the same trends as the Courteau and PW samples.

3 BEST FIT MODELS

3.1 Fits to disk models within NFW profiles

Since we use the observed (stellar) scale lengths of the baryonic disk (R_d), the free parameters in our model are: M_{200}, f_d and c. For each galaxy rotation curve we explore the entire likelihood surface within the following boundaries: $10^9 < {\rm M}_{200}/{\rm M}_\odot < 7\times10^{13}$, $0.1 < c < 100$ and $0.001 < f_d < 0.36$. The choice of the boundaries is justified as follows: for M_{200} by the typical velocities at large radii in the sample, for c by theoretical ansatzs given by N–body simulations and analytic predictions (e.g., MMW); and finally for f_d a realistic upper bound can be given by nucleosynthesis constraints on the baryon fraction $f_d \sim 0.2$ (e.g. Jaffe et al (2001); Efs-

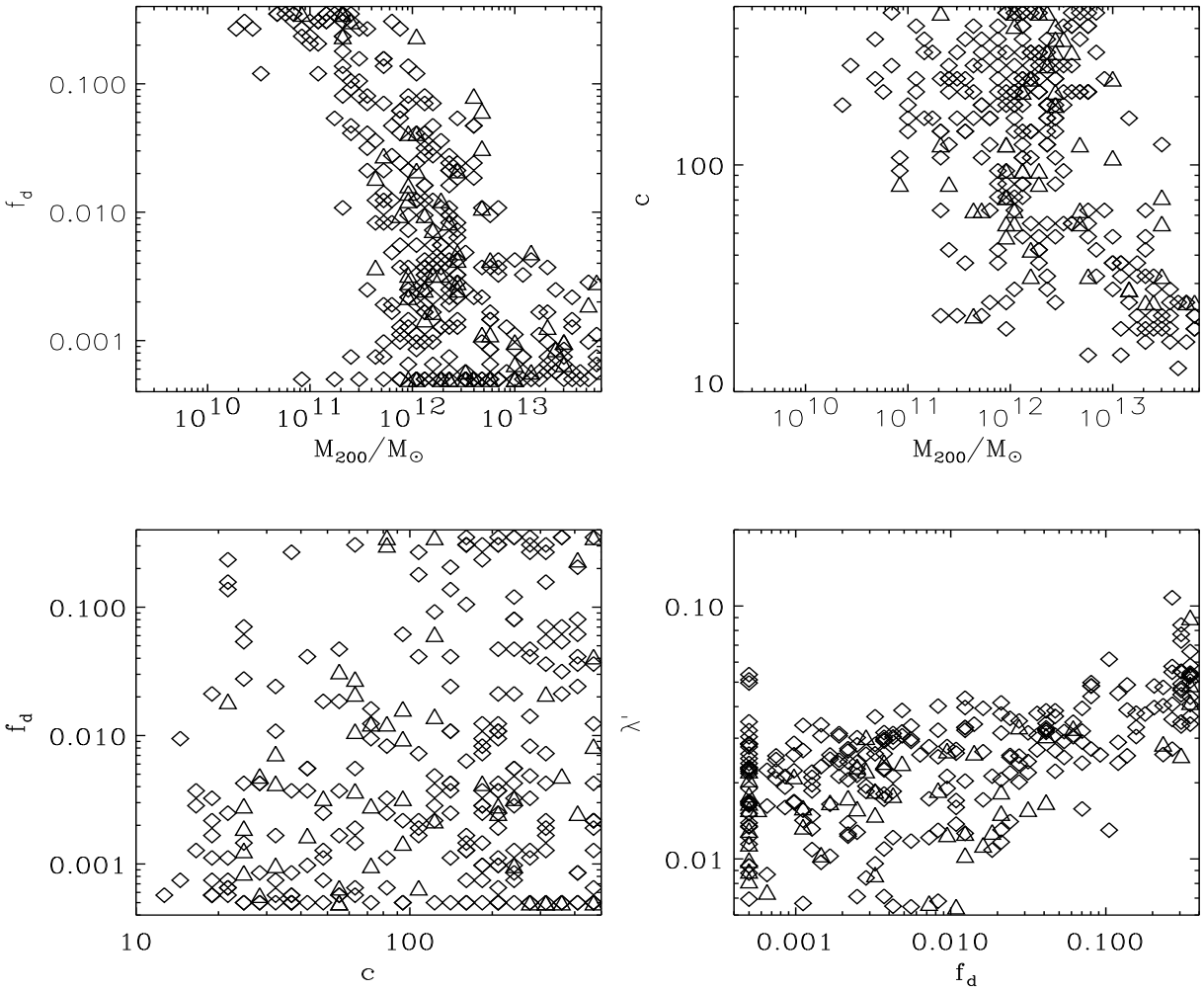

Figure 3. Pseudo-isothermal model. Same as fig. 1 but when using the pseudo-isothermal dark matter halo. Note the similarity with fig. 1.

tathiou et al. (2001)); a realistic lower bound is more difficult to set, but it is reasonable to believe that at least few percent of the baryons in the halo cool to form the disk. We set a higher value $f_d = 0.36$ and a lower value of $f_d = 0.001$ to explore parameter space more fully. The best fitting model is then obtained by using a standard inverse variance weighted χ^2 minimization[1]. We compute the value of χ^2 on the entire grid of points to ensure that we converge on a global, rather than local, minimum in χ^2. The discreteness of points in our solution reflects the finite spacing of our grid.

Figure 1 shows the position of each galaxy for all the projections of the three dimensional parameter space (M_{200}, f_d and c). In addition, for the best fitting values of M_{200}, f_d and c we have computed λ' and plot it against f_d.

For 122 galaxies out of the 362 the χ^2 minimization procedure does not find a global minimum within the boundaries for the disk parameters. This means that for $\sim 1/3$ (i.e., 34%) of the galaxies in the sample the model with a NFW profile for the dark matter fails to reproduce the observed rotation curve. This is in agreement with a previous study by van den Bosch & Swaters (2001). They analyze (with a different procedure and different modelling assumptions from ours) 20 rotation curves of late type dwarfs and find that for 6 of these galaxies (i.e., 30%) no meaningful fit can be obtained. It is important to note that our analysis uses a different approach, a much larger sample of galaxies that is not limited to dwarfs, and still concludes that the same percentage of galaxies are well fitted by a CDM profile.

There are some correlations among disk parameters worth commenting on. The top-left panel of fig. 1 shows an anti-correlation between M_{200} and f_d, with a clear zone of avoidance for low masses and low spins (we discuss the significance and possible physical origin of this zone of avoidance in Verde, Oh & Jimenez (2002)).

The top-right panel of fig. 1 shows that low mass halos have on average higher concentration parameters than massive halos, in agreement with theoretical predictions. This is not surprising since in hierarchical CDM models low mass

[1] The best fitting model to all 400 rotation curves can be found at `http://www.physics.rutgers.edu/~raulj/rot/roti.ps (rotipseu.ps)`

halos form at higher redshift than massive halos. The solid and dashed lines in the top right panel of fig. 1 show the median $M-c$ relation predicted from numerical simulations (Bullock et al. (2001) figs. 4 and 5) for low density and high density environments respectively. Although the recovered distribution of c vs. M_{200} seems to show a somewhat steeper decline of c with increasing M_{200} (in agreement with the findings of van den Bosch, Burkert & Swaters (2001); van den Bosch & Swaters (2001) for 14 dwarf galaxies), it is difficult to draw a definitive conclusion due to the scatter in the theory prediction (simulations show a 30% scatter around this median relation) and in the recovered correlation. The overall distribution of halo concentrations is in reasonable agreement with ΛCDM predictions. This is more clearly seen in the left panel of fig. 2 where the theoretical predictions by Jing (2000) are overplotted as a thick line on the distribution of c (obtained from those galaxies for which a meaningful fit was found). Maybe more interesting is the fact that very few galaxies are found to have values of c below the theoretical predictions. The small tail of 20 galaxies with $c < 0.3$ is mostly due to 14 galaxies for which $f_d > 0.2$, i.e., above the value allowed by nucleosynthesis. For these galaxies the best fit parameter combination is thus unphysical. In §4 we will argue that this might be due to limitations of our model for the rotation curves.

The bottom-left panel shows that there is no evidence for a correlation between f_d and c. On the other hand (bottom-right panel) there is a clear correlation between λ' and f_d. This is in agreement with that found by Burkert (2000) (the solid line shows his best least square fit to the data) and van den Bosch, Burkert & Swaters (2001) but for only 14 dwarf galaxies. This is puzzling because cosmological models do not predict any correlation between λ (where $\lambda' = j_d/f_d\lambda$) and f_d.

Burkert (2000) points out that this correlation can arise because of a correlation between the specific disk angular momentum (j_d/f_d) and f_d. If baryons that make up the disk cooled from the inside out, the outermost rings of the disk, that contain most angular momentum, cooled later; thus predicting a correlation with a slope very close to that observed. In this scenario the total specific angular momentum of the disk should be significantly smaller than that of the dark matter, since most of the galaxies have f_d below nucleosynthesis value, but this seems not to be the case for the 14 galaxies used in the analysis (van den Bosch, Burkert & Swaters 2001; Burkert 2000).

On the right panel of fig. 4 we show the distribution of λ' for galaxies of our larger sample for which a meaningful fit was found. Also plotted as a solid thick line is the theoretical prediction (Bullock et al. 2001) for the distribution of λ found in N-body simulations (which is very similar to that predicted by linear theory (Heavens & Peacock 1988)). Although the agreement is reasonable, there is a tail of galaxies for which the recovered λ' is below the predictions.

Burkert (2000) did not find this, but this may be due to the fact that the galaxies in the sample of van den Bosch, Burkert & Swaters (2001) are LSB's so they are selected to have high spin (Jimenez et al. 1998).

We argue that the most significant feature of the bottom-right panel of figure 1 is the lack of galaxies above the solid line (what we call zone of avoidance). Many different effects might be at play here: disks in the bottom right portion of the plot may be unstable to bulge formation and become bulge-dominated; disks may form preferentially out of low angular momentum gas, which settles in the center first; finally for some combinations of the parameters disks might fail to trigger star formation. In Verde, Oh & Jimenez (2002) we discuss in more detail the origin of the zone of avoidance.

In Appendix II, we explore the degeneracies between model parameters. Although we find that there should be no significant degeneracies between model parameters for most of these high-quality rotation curves, we find that for the lowest quality rotation curves, significant degeneracies develop. The degeneracies have almost exactly the same direction as the 3 correlations recovered from the data. We therefore caution the reader that the correlations between model parameters seen above maybe the result of parameter degeneracies if there are systematic errors in the rotation curves or the quoted errors have been underestimated.

3.2 Fits to disk models within a Pseudoisothermal halo

We fit the pseudoisothermal halo model of §2.1 to the same set of galaxies as above using the same inverse variance weighted χ^2. Our aim is two-fold: first to see if the same correlations among the parameters found for the NFW profile still hold for this new profile and second, to investigate the distribution of core sizes.

We find that, for this dark matter profile model, for 114 galaxies out of the 362 (i.e. 32%) the χ^2 minimization procedure does not find a global minimum within the boundaries.

Figure 3 shows the location of galaxies for the projections of the three dimensional parameter space (M_{200}, f_d, c), where $c \equiv R_{200}/r_c$. As for the NFW profile, there is a clear anti-correlation between f_d and M_{200} and the same zone of avoidance. In Verde, Oh & Jimenez (2002) we discuss in detail the physical origin of this zone of avoidance. Here we only point out that this zone of avoidance seems to be independent of the shape of the dark matter profile.

There is no evidence for a correlation between f_d and c. As for the NFW profile we can now use the best fitting values of (M_{200}, f_d and c) to compute the value of λ' using eqs. 19 and 20 from Appendix I. There is a clear correlation between f_d and λ' (bottom right panel of fig. 3), very similar to that found for the NFW model (fig. 1). The distribution of λ' for the whole sample is shown on the right panel of fig. 4; the thick solid line is the theoretically predicted value. Although the theoretical prediction is obtained from numerical simulations, where the dark matter halo profile is closer to the NFW, there is reasonable agreement. This is not surprising since the N-body predictions are very similar to the linear theory ones, and if halos were isolated (i.e., no further merging after formation) they would be well approximated by isothermal spheres (e.g., Gunn & Gott (1972)).

The upper-right panel shows that most galaxies in the sample have $c = R_{200}/r_c$ larger than 20, already pointing to small sizes of the cores. This is better illustrated in the left panel of fig. 4, where we show the histogram of R_{200}/r_c for the galaxies for which meaningful fit are obtained. There is a sharp cut–off at $R_{200}/r_c \sim 16$, with 70% of the galaxies having $R_{200}/r_c > 100$. This implies that the size of dark

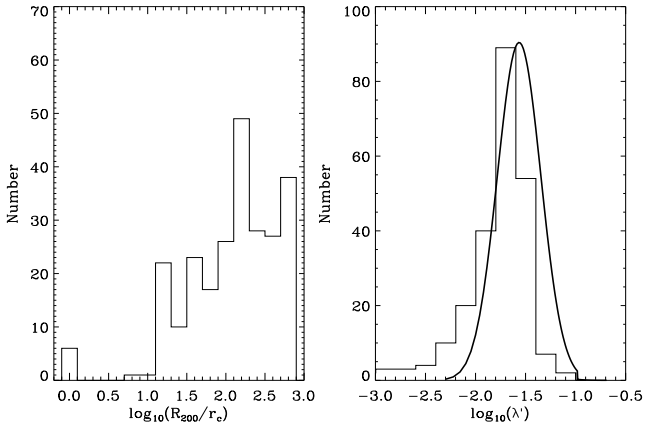

Figure 4. Pseudo-isothermal model. Left panel: distribution of the concentration parameter $c = R_{200}/r_c$ for the pseudo-isothermal dark halo. Note the sharp cut-off at $c = 16$, 70% galaxies in the sample have $c > 100$, i.e. 70% of galaxies have cores with sizes below 1% of the dark halo virial radius. Right panel: the distribution of λ'. The continuous line is the numerical simulations prediction (see text for more details).

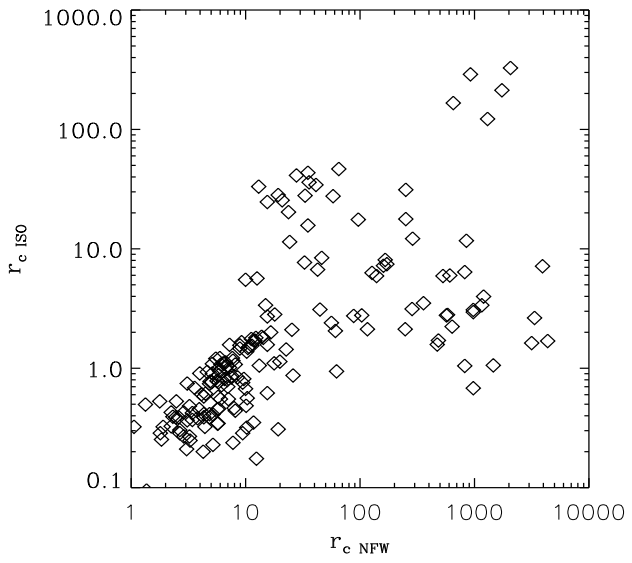

Figure 5. The size of the core radius in the pseudo-isothermal model compared to the break radius in the NFW model. Note that the former is 10 times smaller than the latter and that 70% of the sample has cores below 2 kpc.

matter cores is modest, about 6% of the virial radius or smaller.

4 GENERAL CONSIDERATIONS

From the recovered best fitting disk parameters in the context of the 2 models (NFW profile and pseudo-isothermal profile) we can draw some general conclusions. First of all, the correlations between c and M_{200}, f_d and M_{200} and f_d and λ' are quite similar for the two dark matter profiles: these correlations and the zone of avoidance in the different projections of the three dimensional parameter space (M_{200}, c, f_d) seem to be independent from the shape of the dark matter profile. The disk parameter correlations we find from this large (362 galaxies) and diverse sample of galaxies are in agreement with those found from previous studies that involved much smaller samples (~ 20) and only dwarf or LSBs galaxies (Burkert 2000; van den Bosch, Burkert & Swaters 2001).

Both NFW and pseudoisothermal profiles are *good fits to about 70% the rotation curves*. For the NFW profile we find no meaningful fit for 34% of the galaxies (122 out of 362), while for the pseudoisothermal profile we find no meaningful fit for 32% (114 out of 362). We do not expect to find that the model provides a good fit for all the galaxies in the sample: galaxies might be more complicated than our model for the rotation curves. In fact some rotation curves show strong evidence for spiral arms and bars in the rotation pattern, and we have not attempted to model any bulge or bar component. However, we find that many rotation curves that have no meaningful fit for one dark matter profile are well fitted by the other: for only 52 galaxies (14% of the sample) there is no meaningful fit in either model. These correspond to the poorest quality rotation curves (low spatial resolution and poor spatial coverage, i.e. no flat or inner rotation curve).

Fig. 5 shows that the core radius in the pseudo-isothermal profile ($r_{c\,\mathrm{ISO}}$) is much smaller than the break radius in the NFW profile ($r_{c\,\mathrm{NFW}}$): $r_{c\,\mathrm{ISO}}$ is about 10 times smaller than $r_{c\,\mathrm{NFW}}$. In other words, best fitting models for the dark matter in this sample of galaxies are those with steep dark matter profiles (r^{-1} or steeper), at least down to 6% of the virial radius.

The above considerations lead us to conclude that large dark matter cores (and therefore low central dark matter densities) seem to be excluded. In fig. 6 we show the distribution of central dark matter densities recovered from the best fits to the rotation curves. For the NFW profile model, since the central density is not finite, the densities have been evaluated at $r = 0.5$ kpc. This is comparable to the smallest radius at which the rotation curve can be reliably measured in the samples used in this papers.

The arrow shows the central density (at $r = 0.5$ kpc) inferred by Borriello & Salucci (2001) (see their fig. 5) from 9 galaxies.

We have also selected 37 galaxies (out of the 48 LSBs) analyzed by de Blok et al. (2001), that show indication of a flat core, and computed the distribution of inferred central densities (the 9 galaxies which show no flattening of the profile should have higher central densities). This distribution is shown as the dotted line in fig. 6.

There are a few features worth commenting on. First, the mean density for the pseudo-isothermal profile is slightly lower than that for the NFW profile at 0.5 kpc. The average value of derived central densities for the 27 core galaxies selected from de Blok et al. (2001) is not significantly lower than the average value for the pseudo-isothermal profile. Therefore, there is quite a reasonable agreement for the central densities derived from our model and those derived inverting the Poisson equation in the above LSB galaxies. Of course, the NFW densities will be much higher at radii below 0.5 kpc. Since densities for smaller radii have not been

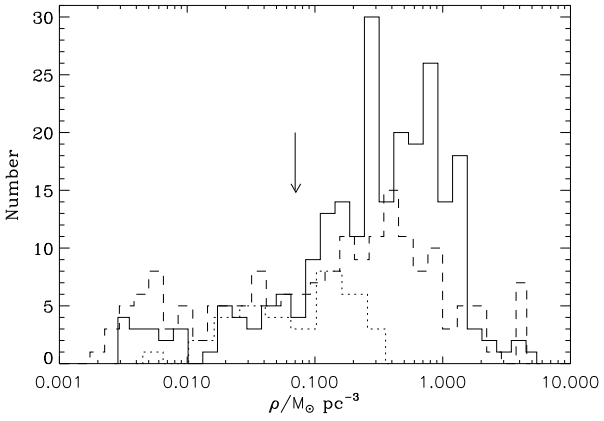

Figure 6. The distribution of central dark matter density for the two profiles at a distance from the center of 0.5 kpc. The dashed line corresponds to pseudo-isothermal dark halos while the solid line corresponds to NFW dark halos. Note the modest density of dark matter. The arrow shows the central density (at $r = 0.5$) inferred by Borriello & Salucci (2001) and the dotted line is the distribution of central densities for 27 galaxies from de Blok et al. (2001) that show a flat core.

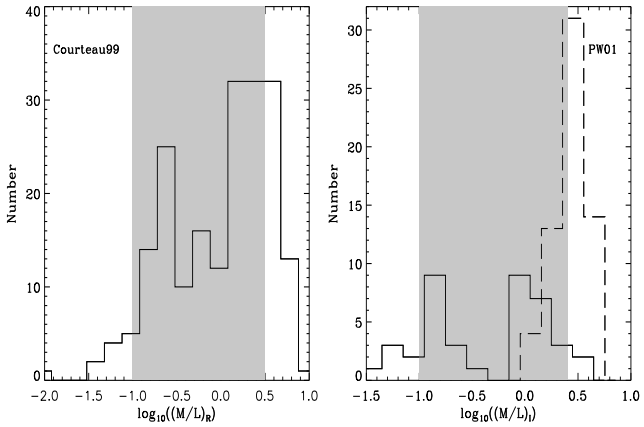

Figure 7. NFW model. The predicted (M/L) in our analysis, using the NFW dark halo profile, for the Courteau and PW samples. The left panel corresponds to the Courteau sample. The right panel shows the histogram for the galaxies in the PW sample as a solid line. The dashed line shows the resulting distribution for the (M/L) ratio assuming a maximum disk model (Palunas & Williams 2000). The gray areas correspond to the allowed values from synthetic stellar populations.

directly derived in a reliable way, it is difficult to assess whether or not the high dark matter densities predicted by the NFW profile are excluded. We simply point out that physical mechanisms that remove efficiently most of the dark matter inside the central kpc from a steep dark matter profile are currently under investigation (Merritt et al. 2002, in preparation; Milosavljevic et al. 2002, in preparation).

4.1 M/L of the sample

A good independent test of the values of the best fit disk parameters (in particular of f_d) recovered from modelling of the rotation curves is a comparison of the baryonic mass-to-light ratios (M/L) inferred from the recovered disk mass $M = f_d M_{200}$ and measured luminosity (L; from photometry) with values predicted by synthetic stellar population models. Stellar synthesis models assume an initial mass function (IMF) and a star formation rate, age and metallicity to uniquely predict the M/L. The IMF is an ansatz which can be guided by observations in the solar neighborhood (e.g., Kroupa (2001)), while the star formation rate, age and metallicity can be inferred with help of the spectrum of the stellar population. In our case, because spectra are not available, we have to make reasonable guesses for these parameters. Once they have been fixed, current stellar synthesis models agree, quite remarkably, in their predictions about the M/L ratio (e.g., Bell & de Jong (2001)). However, uncertainty in the assumptions ultimately limit the precision in the M/L predictions from synthetic stellar population models, leaving a 20-40 % uncertainty. Taking these uncertainties into account, a large disagreement between the M/L recovered from the rotation curve modelling and permitted values from stellar synthesis models, would imply that the modelling of the rotation curves is probably incorrect.

Fig. 7 shows the baryonic M/L ratios derived by using the best fitting model values for M_{200} and f_d for the NFW

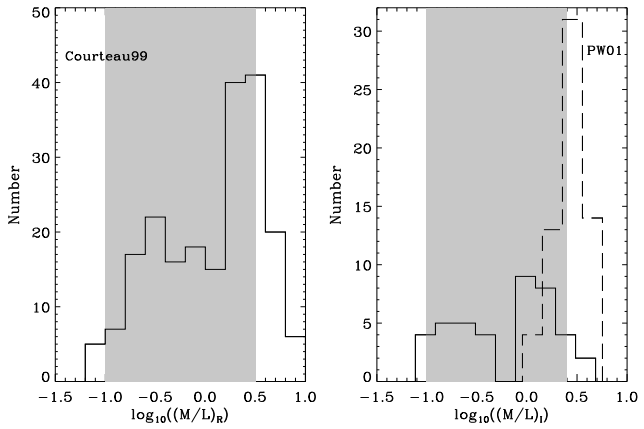

Figure 8. Pseudo–isothermal model. The predicted (M/L) in our analysis and in synthetic stellar populations. The line styles and shaded areas have the same meaning as in fig. 7.

profile (for the 240 galaxies for which meaningful fits were found) and the published values for the reddening-corrected integrated photometry for the Courteau and PW samples (Courteau 1997; Palunas & Williams 2000); Fig 8 shows the distribution of M/L ratios recovered by using the pseudo-isothermal profile model. In both cases, the recovered distribution of M/L is fairly broad.

In both figures, the allowed range of M/L using the synthetic stellar population models developed in Jimenez et al. (1998) are shown as gray areas. This range is obtained by varying $B - R$ (between 0 and 1.5), the IMF (Salpeter; Miller–Scalo) and the star formation history of galaxies (a star formation recipe with a star formation rate $\dot{M}_* \propto \exp(-t/t_*)$, where 3 Gyr $\leqslant t_* \leqslant$ 20Gyr). These assumptions allow $0.1 < (M/L)_{R,I} < 3$ where the subscript R, I refers to the M/L in the R and I bands; the assumed

age of the stellar population has the greatest impact on the derived M/L range, with low values of M/L associated with progressively younger stellar populations.

The M/L derived from the NFW profile show a somewhat broader range than allowed: for the Courteau sample 4% of the galaxies have uncomfortably low M/L while 16% have M/L *larger* than allowed from synthetic stellar populations; for the PW sample 14% have low M/L and 7% have too high M/L. For the pseudoisothermal profile the situation is very similar: for the the Courteau sample 2% of galaxies have low M/L and 17% have too high M/L while for the PW sample 5% have too low M/L and 10% too high.

It is commonly claimed in the literature that NFW fits require M/L ratios which are too low; this is then used as an argument against dark matter profiles with central cusps (de Blok, McGaugh & Rubin 2001). The majority of studies have however focused on LSBs; we find that for HSBs only a small fraction of galaxies have excessively low M/L. Low values of M/L may plausibly be associated with very young stellar populations (e.g., if the last burst of star formation is ~ 1 Gyr old, then $(M/L)_{\rm R,I} \sim 0.1$. Tighter constraints on M/L are only possible with multi-color photometry or ideally, spectroscopy). Note that the distributions of M/L ratios derived from the pseudoisothermal profile are very similar to those derived using the NFW profile (fig. 7 and 8); removing the central dark matter cusp does not change M/L significantly. Thus we conclude that the derived disk mass is fairly independent of the dark matter profile we assume and in broad agreement with values allowed by synthetic stellar population models.

A possible criticism of studying HSB galaxies is that, in contrast to LSBs, the rotation curves of these galaxies are not dark matter dominated. In an extreme case, this would correspond to a maximum disk model, in which the circular velocity is attributable solely to the disk. In this case, we would be completely insensitive to the dark matter profile. The dashed line histograms in the right panels of figures 7 and 8 show the M/L ratio derived by Palunas & Williams (2000) fitting a maximum disk model to their sample. Not surprisingly, their derived average M/L is larger than that of both the NFW and pseudoisothermal profile; however, it is also larger than allowed by the synthetic stellar population models. The Sa-Sd disk galaxies in the Palunas & Williams (2000) sample have $B-R < 1.2$, which fairly robustly implies $(M/L)_{\rm R,I} < 2.5$. The M/L ratios implied by the maximum disk models are much larger: they are more typically associated with ellipticals.

4.2 Low recovered disk mass fractions f_d

It is worth commenting on the low values of f_d we obtain. For both the NFW and pseudo-isothermal fits, we often obtain values of f_d as low as $f_d \sim 10^{-3}$, even for $M_{200} \sim$ few $\times 10^{12} M_\odot$. This is implausibly low: it implies only $\sim 1\%$ of the baryons in the halo cool to form the disk. It is difficult to think of any feedback mechanism (e.g., supernovae explosions) which could have such an extreme effect in inhibiting cooling or expelling baryons from the disk (e.g., Efstathiou (2000)). A possible mechanism that can considerably reduce the amount of gas in disk galaxies is RAM pressure stripping (Quilis, Moore & Bower 2000). However this mechanism works only on galaxies orbiting in clusters. We do not have extended information about the environment of the galaxies from our sample, but very low values of f_d are found also from analysis of LSB's galaxies (e.g. van den Bosch, Burkert & Swaters (2001)) that are not found orbiting clusters. Thus the ram pressure stripping mechanism seems not to be responsible for the low values of f_d we recover.

These very low values of f_d are also responsible for the tail of low M/L galaxies in figures 7 and 8.

At present, we regard these low values of f_d as pointing toward some inadequacy of the simple disk-halo model, or the assumed form of the dark matter profile. On the other hand, the high mass end of the galaxy mass function is dominated by elliptical galaxies and it is not inconceivable that we are selecting only those dark halos that manage to form a disk.

Since the value of f_d mainly affects the inner part of the rotation curve, we may ask: how should the dark matter profile be modified so that the recovered f_d is more meaningful? It is clear that dark matter density in the center needs to be reduced. However, as discussed above, the best fit model for the pseudoisothermal profile has very small cores (and a steeper $-r^{-2}-$ slope outside).

We are investigating possible physical mechanisms within the CDM paradigm that can achieve such result, thus decreasing substantially the dark matter content of a NFW halo within the inner kpc (Merritt et al. 2002, in preparation; Milosavljevic et al. 2002, in preparation).

5 CONCLUSIONS

We have analyzed a large set of high spatial resolution rotation curves of galaxies with the goal of determining the model parameters for a disk embedded within a cold dark matter (CDM) halo that we have modeled in two ways: either with a NFW profile or a pseudo-isothermal profile. To this aim we have developed the expression for the rotation curve of an exponential disk embedded in a pseudoisothermal halo (Appendix I).

Our study differs from previous work in two respects. Firstly, we use optical rotation curves rather than HI rotation curves, so the rotation curves we use are free from beam smearing and have smaller errors and higher spatial resolution. Secondly, while many studies have focused on relatively small samples of dwarfs, we use a large sample (400 galaxies) spanning a wide range in luminosity and surface brightness.

We find that the NFW profile provides a good fit to 66% of the galaxies in the sample (in agreement with previous studies, van den Bosch & Swaters (2001)) that were based on few (20) dwarf galaxies), with a distribution of recovered concentration parameters and spin parameters broadly consistent with that predicted by CDM numerical simulations. When the sample is fitted with an isothermal profile with a core, 68% of the galaxies are well fitted within this model and the best fit model favors cores with small sizes (almost all have $r_c < 0.06 R_{200}$ and $\sim 70\%$ have $r_c < 0.01 R_{200}$). However, we find that many rotation curves that have no meaningful fit for one dark matter profile are well fitted by the other: for only 52 galaxies (14% of the sample) there is no meaningful fit in either model. These largely comprise low

quality rotation curves. Our findings are consistent with the inner dark matter profiles being steep (slope of -1 or steeper) down to radii that are few percent of the virial radius. Large dark matter cores (and therefore low central dark matter densities) seem thus to be excluded.

Numerical SPH simulations of disk formation within dark halos find that disks loose a significant fraction of their angular momentum if: 1) the dark matter profile is steep in the center and 2) the baryons settle in right after virialization (Navarro & Steinmetz 2000a). On the other hand, we recover steep dark matter profiles and no significant loss of angular momentum. There are several routes to explain this. Some authors have pointed out that if baryons are allowed to settle well after virialization of the halo (e.g. Sáiz et al. (2001)), then there is no significant loss of angular momentum. Another possibility to consider is that current hydrodynamical simulations lack the resolution to simulate a multi-phase interstellar medium and also to follow the detailed formation of giant molecular clouds, and therefore the sites of star formation, within the settling disk. It is therefore not clear that current simulations contain all the physical ingredients needed to simulate the complex process of baryons cooling down into a disk.

In both models, for the galaxies that have meaningful fit to the rotation curves, the recovered baryonic mass to light ratios are broadly in agreement with predictions from synthetic stellar populations.

From this large sample of galaxies we find several correlations among the best fitting model parameters and some regions in the parameters space that are not populated, we refer to those regions as zone of avoidance. These correlations an zone of avoidance are remarkably similar in both profiles and do not change when the rotation curves are fitted by a model with three free parameters or with four free parameters. In particular we find a strong correlation between the disk mass fraction and the spin parameter for different kind of galaxies (HSBs and LSBs), in good agreement with findings of previous studies that involved only few dwarf LSBs galaxies. These correlations may be a result of parameter degeneracies if errors in the rotation curve have been underestimated; otherwise, they could have a physical origin.

When fitting the sample with the NFW profile we obtain that for the 66% of galaxies for which meaningful fits to the rotation curves are found, the distribution of concentrartion parameters is in good agreement with predictions from N-body simulations. Also, the distribution of disk spin parameters is in broad agreement with the distribution of spin parameters for the dark matter predicted from N-body simulations and linear theory, but with a small tail at low spins.

The primary motivation in previous work of studying the rotation curves of dwarfs and/or LSB's was that they would be dark matter dominated. Although it is quite plausible, this claim must be taken with caution. In fact, our analysis of HSB and more luminous galaxies, as we have seen, yields values for the baryonic disk mass fraction very similar to previous analysis of dwarfs; a naive interpretation of rotation curve fits alone would lead us to claim these galaxies as dark-matter dominated as well. In Appendix II, we analyze the LSB sample of McGaugh, Rubin & de Blok (2001) and find that a somewhat larger fraction of them cannot be fit by NFW profiles, $\sim 57\%$ as opposed to $\sim 33\%$ for the entire sample (those which do fit have somewhat low but theoretically plausible concentration parameters c). This difference may be a 1 σ statistical fluctuation (there are only 26 LSBs in the sample), it may reflect the greater fidelity of LSB rotation curves to the true underlying dark matter distribution, or it may perhaps be due to a systematic difference in the dark matter profile of halos which undergo greater tidal torquing. On the other hand, for the pseudoisothermal model, only one LSB has $f_d > 0.2$. This seems to indicate that LSBs are indeed fitted better with a dark matter core. For the LSB sample, 9 galaxies have dark matter cores with sizes below 1.5 kpc and 16 below 3 kpc. This is in fair agreement with our previous findings that the size of the dark matter core is modest. It is also in agreement with the dark matter core size inferred from inverting the Poisson equation using the observed rotation curve (de Blok et al. 2001). Ultimately, our sample choice involves a trade-off: we gain increased precision in the rotation curve (which breaks parameter degeneracies) and a much larger sample encompassing a much broader class of galaxies, but also acquire a somewhat larger uncertainty in the disk contribution to the rotation curve.

In general, LSB galaxies tend to have higher values of λ' for a given f_d and lower values of c for a given mass than HSB galaxies (see Appendix II). This supports the view that the dark matter profile of LSBs might reflect an enviroment in which dark halos undergo a higher tidal torque.

If the M/L of the disk was well constrained, this ambiguity can be eliminated: it would be possible to subtract the disk contribution to the rotation curve and recover directly the inner profile of the dark halo by inverting the Poisson equation (e.g., de Blok et al. (2001)). The M/L can be constrained from multi-color photometry or even better, high S/N spectra of the stellar population in galaxies (extending as close as possible to the K band) together with high-spatial resolution rotation curves especially of the inner 1-2 Kpc. A more detailed treatment of this issue will be presented in a forthcoming paper.

ACKNOWLEDGMENTS

We thank David Spergel for insightful comments and stimulating discussions. We also thank Povilas Palunas and Ted Williams for making available their rotation curve sample. LV is supported in part by NASA grant NAG5-7154. SPO is supported by NSF grant AST-0096023. LV and RJ thank the TAPIR group at Caltech for hospitality. This research has made use of NASA's Astrophysics Data System Abstract Service.

REFERENCES

Avila-Reese V., Firmani C., 2000, Revista Mexicana de Astronomia y Astrofisica, 36, 23
Bell E. F., de Jong R. S., 2001, ApJ, 550, 212
Binney J., Tremaine S., 1987, Galactic dynamics. Princeton, NJ, Princeton University Press, 1987, 747 p.
Bode P., Ostriker J. P., Turok N., 2001, ApJ, 556, 93
Borriello A., Salucci P., 2001, MNRAS, 323, 285

Bullock J. S., Dekel A., Kolatt T. S., Kravtsov A. V., Klypin A. A., Porciani C., Primack J. R., 2001, ApJ, 555, 240
Bullock J. S., Kolatt T. S., Sigad Y., Somerville R. S., Kravtsov A. V., Klypin A. A., Primack J. R., Dekel A., 2001, MNRAS, 321, 559
Burkert A., 2000, astro-ph/0007047
Cen R., 2001, ApJL, 546, L77
Colombi S., Dodelson S., Widrow L. M., 1996, ApJ, 458, 1
Courteau S., 1997, AJ, 114, 2402
Dalcanton J. J., Bernstein R. A., 2000, in Dynamics of Galaxies: from the Early Universe to the Present, 15th IAP meeting held in Paris, France, July 9-13, 1999, Eds.: Francoise Combes, Gary A. Mamon, and Vassilis Charmandaris ASP Conference Series, Vol. 197 p. 161
Dalcanton J. J., Spergel D. N., Summers F. J., 1997, ApJ, 482, 659
de Blok E., McGaugh S., Rubin V., 2001, astro-ph, 0107366
de Blok W. J. G., McGaugh S. S., Bosma A., Rubin V. C., 2001, ApJL, 552, L23
Efstathiou G., 2000, MNRAS, 317, 697
Efstathiou et al. G., 2001, astro-ph/0109152
Firmani C., Avila-Reese V., 2000, MNRAS, 315, 457
Goodman J., 2000, New Astronomy, 5, 103
Gunn J., Gott R., 1972, ApJ, 176, 1
Heavens A. F., Peacock J. A., 1988, MNRAS, 232, 339
Hu W., Barkana R., Gruzinov A., 2000, Physical Review Letters, 85, 1158
Jaffe et al A. H., 2001, Physical Review Letters, 86, 3475
Jimenez R., Heavens A., Hawkins M., Padoan P., 1997, MNRAS, 292, L5
Jimenez R., Padoan P., Matteucci F., Heavens A. F., 1998, MNRAS, 299, 123
Jing Y. P., 2000, ApJ, 535, 30
Kamionkowski M., Liddle A. R., 2000, Physical Review Letters, 84, 4525
Keeton C. R., 2001, ApJ, 561, 46
Klypin A., Kravtsov A. V., Valenzuela O., Prada F., 1999, ApJ, 522, 82
Kroupa P., 2001, MNRAS, 322, 231
Lahav et al. O., 2001, astro-ph/0112162
McGaugh S., Rubin V., de Blok E., 2001, astro-ph, 0107326
McGaugh S. S., de Blok W. J. G., 1998, ApJ, 499, 41
Mo H. J., Mao S., White S. D. M., 1998, MNRAS, 295, 319
Moore B., Ghigna S., Governato F., Lake G., Quinn T., Stadel J., Tozzi P., 1999, ApJL, 524, L19
Navarro J., 1998, astro-ph/9807084
Navarro J. F., Frenk C. S., White S. D. M., 1997, ApJ, 490, 493
Navarro J. F., Steinmetz M., 2000a, ApJ, 538, 477
Navarro J. F., Steinmetz M., 2000b, ApJ, 528, 607
Palunas P., Williams T. B., 2000, AJ, 120, 2884
Peacock et al J. A., 2001, Nature, 410, 169
Phillips J., Weinberg D. H., Croft R. A. C., Hernquist L., Katz N., Pettini M., 2001, ApJ, 560, 15
Quilis V., Moore B., Bower R., 2000, Science, Volume 288, Issue 5471, pp. 1617-1620 (2000)., 288, 1617
Sáiz A., Domínguez-Tenreiro R., Tissera P. B., Courteau S., 2001, MNRAS, 325, 119
Salucci P., 2001, MNRAS, 320, L1
Salucci P., Burkert A., 2000, ApJL, 537, L9
Somerville R. S., Primack J. R., 1999, MNRAS, 310, 1087
Spergel D. N., Steinhardt P. J., 2000, Physical Review Letters, 84, 3760
Swaters R. A., Madore B. F., Trewhella M., 2000, ApJL, 531, L107
van den Bosch F. C., 2000, ApJ, 530, 177
van den Bosch F. C., Burkert A., Swaters R. A., 2001, MNRAS, 326, 1205
van den Bosch F. C., Robertson B. E., Dalcanton J. J., de Blok W. J. G., 2000, AJ, 119, 1579
van den Bosch F. C., Swaters R. A., 2001, MNRAS, 325, 1017
Verde L., Oh S. P., Jimenez R., 2002, astro-ph
Verde et al. L., 2001, astro-ph/0112161

APPENDIX I: ROTATION CURVE FOR PSEUDO–ISOTHERMAL PROFILE

In this Appendix, we derive three relations used in the text for the pseudo–isothermal halo profile: (i) the rotation curve of the pseudo-isothermal sphere, equation (12), (ii) the relation between the finite central density and the concentration parameter ($c \equiv r_{200}/r_c$), equation (15) ; (iii) a fitting formula for the disk scale-length R_d as a function of the halo mass and core-radius (M_{200}, r_c), and the disk mass fraction and spin (f_d, λ') assuming angular momentum is conserved, equation (20).

Starting from

$$\rho(r) = \frac{\rho_0}{1 + (r/r_c)^2} \tag{10}$$

we obtain

$$M(r) = \int_0^r r'^2 \rho(r') dr = \rho_0 4\pi r_c^2 \left[r - r_c \mathrm{arctan}\left(\frac{r}{r_c}\right)\right] \tag{11}$$

thus

$$V_{CDM}^2(r) = 4\pi G \rho_0 r_c^2 \left[1 - \frac{r_c}{r}\mathrm{arctan}\left(\frac{r}{r_c}\right)\right] \tag{12}$$

and

$$M_{200} = \rho_0 4\pi r_c^3 \left[c - \arctan(c)\right] \tag{13}$$

where $c = R_{200}/r_c$. Since by definition

$$\frac{M_{200}}{4/3\pi R_{200}^3} \equiv 200\rho_{\rm crit} \tag{14}$$

we have that

$$\rho_0 = \frac{200}{3}\rho_{\rm crit}\frac{c^3}{c - \arctan(c)}. \tag{15}$$

The disk scale length R_d is obtained as follows. From the definition of the spin parameter λ, the total angular momentum of the dark matter halo is:

$$J = \frac{\lambda}{|E|^{1/2} G^{-1} M_{200}^{-5/2}}, \tag{16}$$

where E is the total energy of the halo. The total angular momentum of the disk J_d is given by:

$$J_d = 2\pi \int_0^{r_\infty} V(r)\Sigma(r) r^2 dr \equiv j_d J \tag{17}$$

where $\Sigma(r) = \Sigma_0 \exp[-r/R_d]$, and the central density is

$\Sigma_o = f_d M_{200}/(2\pi R_d^2)$. The total energy E can be obtained through the virial theorem $2K + U = 0$, where k denotes the kinetic energy K and U the potential energy: $E = k + U = U/2$, thus,

$$E = -\frac{1}{8\pi G}\int_0^{R_{200}} \left(\frac{GM(r)}{r^2}\right)^2 4\pi r^2 dr \quad (18)$$
$$= -\rho_0^2\pi^2 8 G r_c^4 \int_0^{R_{200}} dr \left[1 - \frac{r_c}{r}\arctan\left(\frac{r}{r_c}\right)\right]^2$$

Using equations (16)–(19) we obtain the following equation:

$$q \equiv \frac{\lambda' G^{1/2} M_{200}^{3/2}}{r_c^2\sqrt{|E|4\pi\rho_0}} = Y^2\int_0^\infty \sqrt{1 - \frac{\arctan(x)}{x}}x^2\exp(-xY)dx \quad (19)$$

where $\lambda' = \lambda j_d/f_d$ and $Y = r_c/R_d$. Equation (19) can easily be solved numerically for Y and thus R_d. We give here a fitting formula that is good to $\lesssim 5\%$:

$$Y = \frac{\alpha}{q^\beta + \gamma q^\delta} \quad (20)$$

where q is defined in eq. 19, $\alpha = 2.3$, $\beta = 0.4745$, $\gamma = 0.85$, $\delta = 1.045$. Equation (20) gives an expression for the disk scale-length R_d for a disk embedded in a pseudo-isothermal sphere.

APPENDIX II: FIT TO 4 PARAMETER MODELS

In this Appendix we explore how a model with four free parameters (M_{200}, f_d, λ and c), i.e. without fixing R_d from observations, fares against the three free parameters model used in the paper. This is interesting for two reasons: it allows us to estimate how much worse the parameter estimation becomes when adding an extra free parameter and allows us to assess the robustness of the zones of avoidance. As in the paper we study both a NFW and a pseudo-isothermal dark matter halo. We also include the LSB sample and show that the trends for parameter correlations for LSBs are the same as for the Courteau and PW samples (HSBs).

In this case, for each galaxy rotation curve we explore the entire likelihood surface within the same limits as the three free parameter model and $0.001 < \lambda' < 0.5$.

In fig. 9 and 10 we show the position of each galaxy in all six projections of the four dimensional space $(f_d, M_{200}, \lambda', c)$, for the NFW and pseudo-isothermal models respectively. Diamonds correspond to galaxies from the Courteau (1997) sample, triangles to galaxies from Palunas & Williams (2000) and squares to the LSB galaxies from McGaugh, Rubin & de Blok (2001).

First we discuss the case of the NFW profile (fig. 9). The same correlations and zone of avoidance are present as in the three free parameter model; for 144 galaxies out of the 400 no fit was found within the boundaries. The upper-left panel of fig. 9 shows the same zone of avoidance (low values of f_d and high values of λ' are avoided) as before and also a similar correlation between f_d and λ' although not as clear as the one in fig. 1.

The change in the resulting distribution of recovered parameters can be seen clearly in the plane $c - M_{200}$. Here a large group of galaxies have recovered values of c and M_{200} in excellent agreement with those found in fig. 1. On the other hand, a clump with unphysical values of $c < 1$ is clearly visible. They correspond to galaxies with unphysically high values of f_d (see the corresponding clump in the $M_{200} - f_d$ plane). About 25% of the rotation curves favours this different solution. These are low spatial resolution rotation curves: their quality is comparable to that of f583-4 shown in fig. 15.

Note that in all 3 cases, the degeneracies between parameters run in almost exactly the same direction as the correlations recovered from the data. These correlations may therefore be the result of parameter degeneracies if errors in the rotation curve have been underestimated.

For the four free parameter case considered here the recovered M/L are slightly broader than for the three free parameter case. This indicates that for this case we are still recovering correctly the mass of the disk. We have computed the M/L for the eight systems in the LSB sample with reliable photometry. For these systems, $M/L = 0.1 - 2.5$ in the B band for both the NFW and pseudo-isothermal profile, in fair agreement with the predictions from synthetic stellar population models.

The recovered parameters for the pseudo-isothermal dark matter halo are shown in fig. 10. Also in this case the zones of avoidance are preserved and the correlations among the different parameters are remarkably similar to those obtained from the three free parameter model. In this case for 141 galaxies out of 400, no fit was found within the boundaries for the parameters.

From fig. 10 it can be seen that LSB galaxies tend to have higher values of λ' for a given f_d and lower values of c for a given mass than HSB galaxies. A similar trend occurs for the NFW profile.

Figure 11 shows the recovered values of R_d in this case plotted against the measured values from the photometry for the two profiles. We see that the disk scale length is very poorly constrained from the rotation curves alone. In particular, for the pseudo-isothermal case the estimated disk scale-length is systematically several times larger than the true disk scale length. This corresponds to inserting a constant surface density sheet over the extent of the rotation curve.

APPENDIX III: DEGENERACIES IN THE MODEL

Similar modelling to that performed here, but with HI rotation curves, has shown that there are serious model degeneracies (e.g., van den Bosch, Burkert & Swaters (2001)). For example, it is common to expect a degeneracy between M_{200} and c (see e.g., de Blok, McGaugh & Rubin (2001)). In this section we argue that the main reason for this is the poor spatial resolution of the HI curves and not the model itself. To demonstrate this we will explore the likelihood surfaces of the 400 NFW fits (same conclusions derived in this section apply to the pseudoisothermal fits). We choose to do this using fits to 4 parameters to demonstrate that even with such a large number of free parameters degeneracies are removed for high-resolution rotation curves. Obviously, for the case of only 3 free parameters, possible degeneracies will be even more restricted.

First, it is useful to look at how the model behaves under

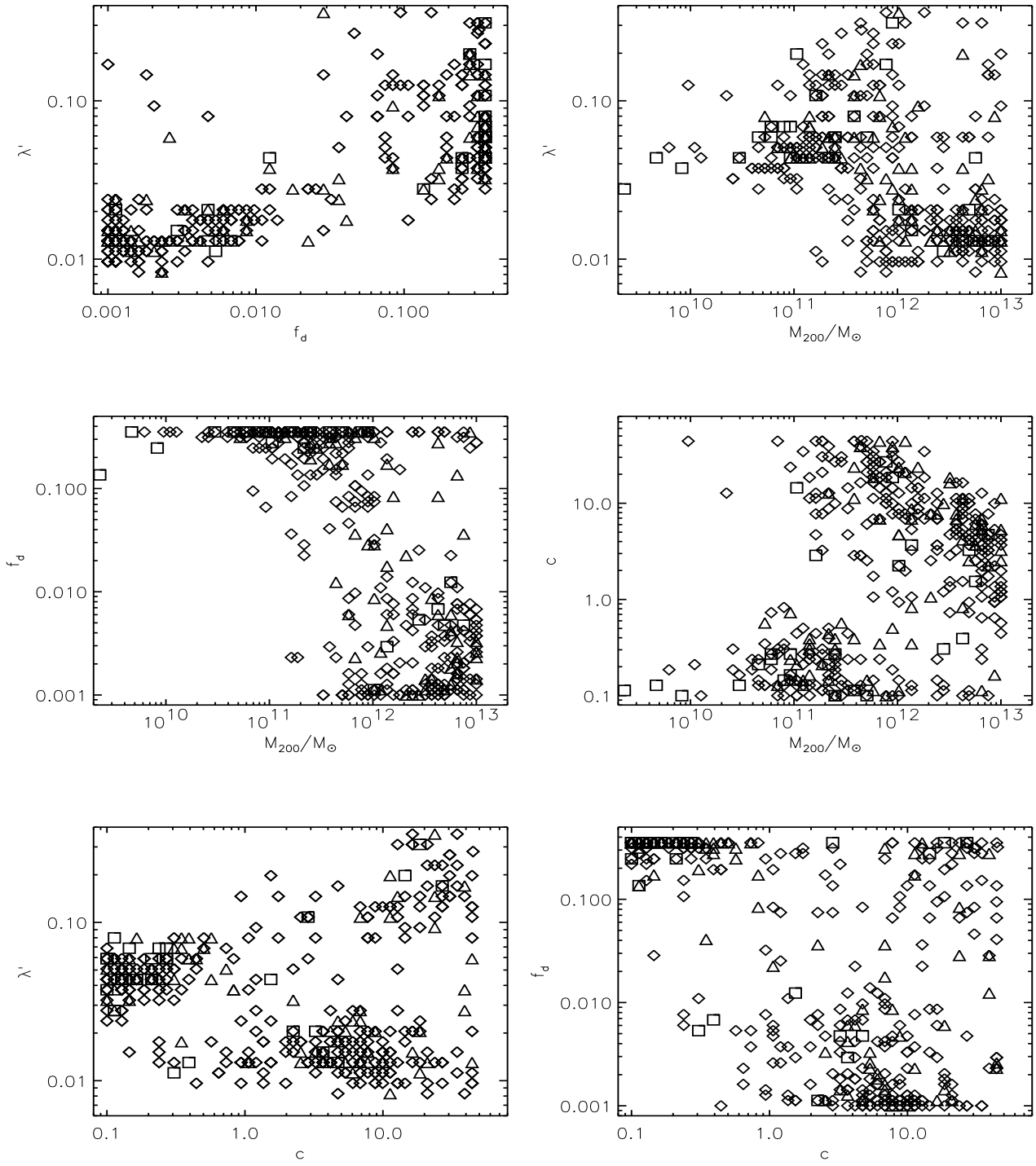

Figure 9. NFW model, four parameters fit. In all six panels diamonds correspond to the Courteau, triangles to the PW and squares to the LSB sample. The correlations between λ and f_d (upper-left panel), M_{200} and f_d (middle-left panel) are very similar to that obtained for the three parameter fit. Note the distribution of c vs. M_{200}.

changes of parameter values. To illustrate this we choose a fiducial model with $(M_{200}, \lambda', f_d, c)$=$(1\times10^{11}$ M$_\odot$, 0.05, 0.01, 10) and explore some of the possible degeneracies present in the rotation curve. To do this we keep two parameters fixed and allow the other two to change from their fiducial value. This results in six possible combinations. There will be degeneracy if in any of these combinations the two rotation curves are indistinguishable. Fig. 12 shows the percentage difference of the rotation curve so obtained with the fiducial model. Note that if the rotation curve is not known to better

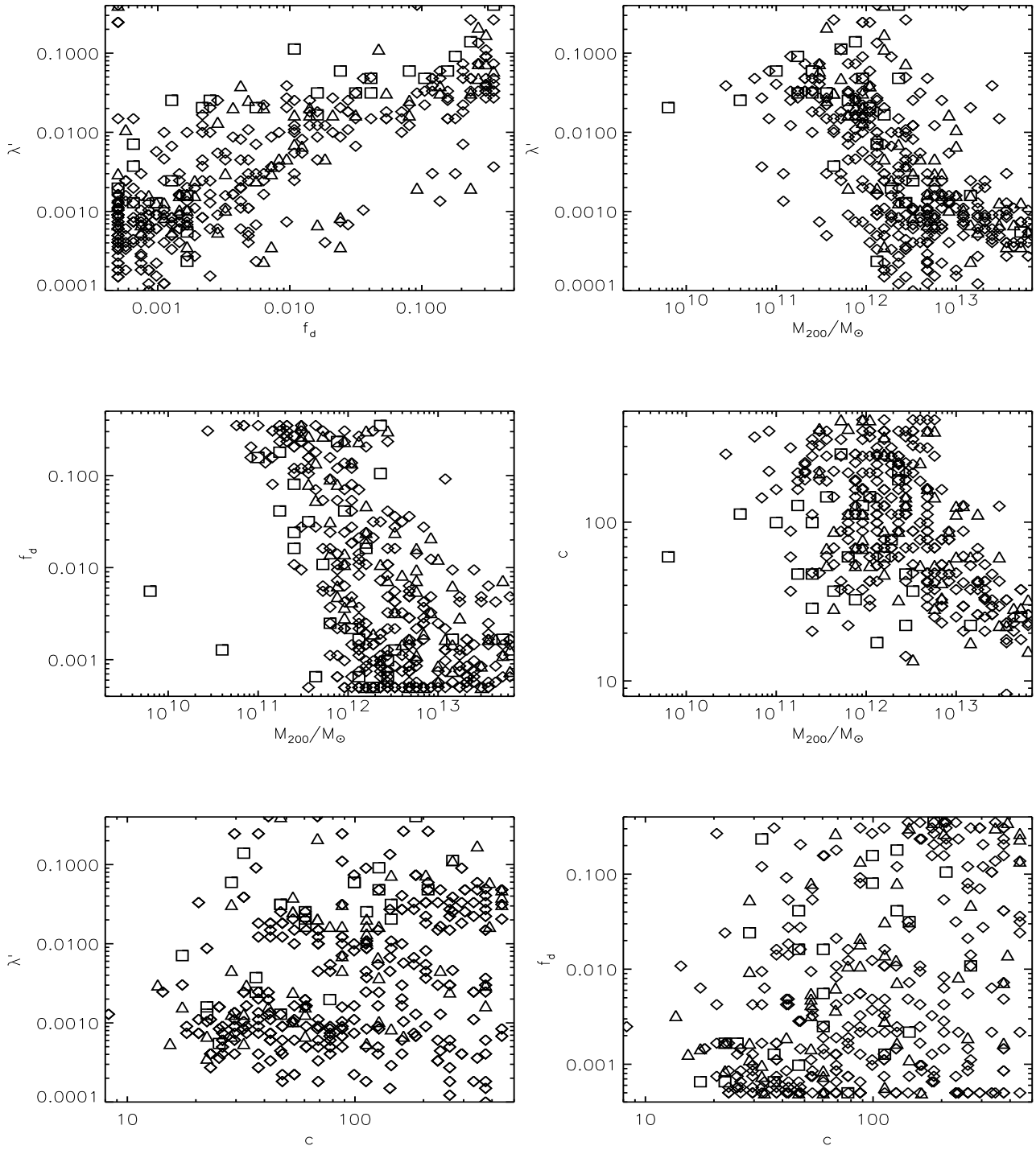

Figure 10. Same as fig. 9 but for the model with disks inside pseudo-isothermal dark halos. Note that the correlations between λ and f_d and between M_{200} and f_d are very similar to those found for the NFW model and to those found for the three parameters fit. Note in the $\lambda' - f_d$ panel that LSBs have higher values of λ' than HSBs for a given value of f_d. Also, in the $c - M_{200}$ panel, LSBs have lower values of c than HSBs for a given mass.

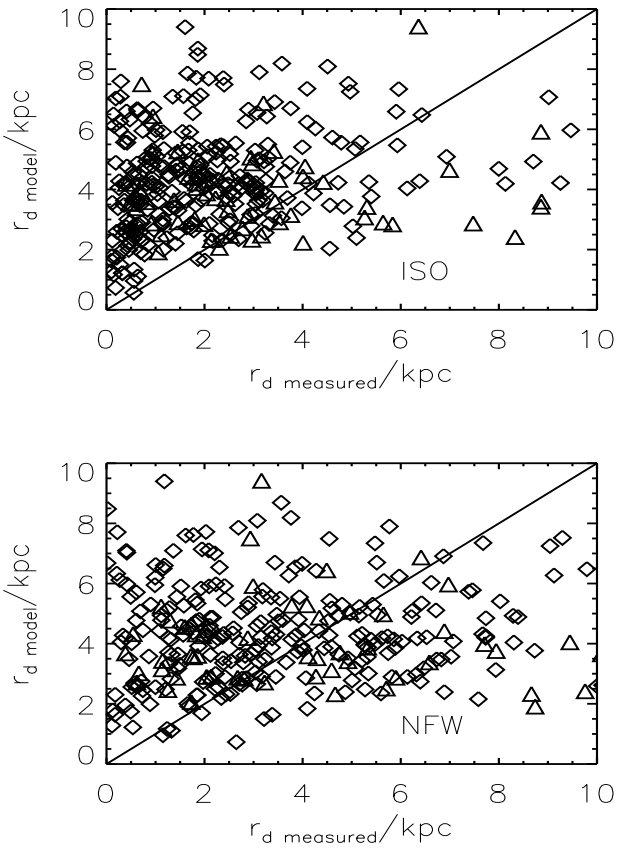

Figure 11. Comparison of the recovered scale-length of the disk, when using a four free parameter model, for the pseudo-isothermal model (top panel) and the NFW model (bottom panel) with the observed stellar scale-lengths. The disk scale-lengths are very poorly constrained from the rotation curve alone.

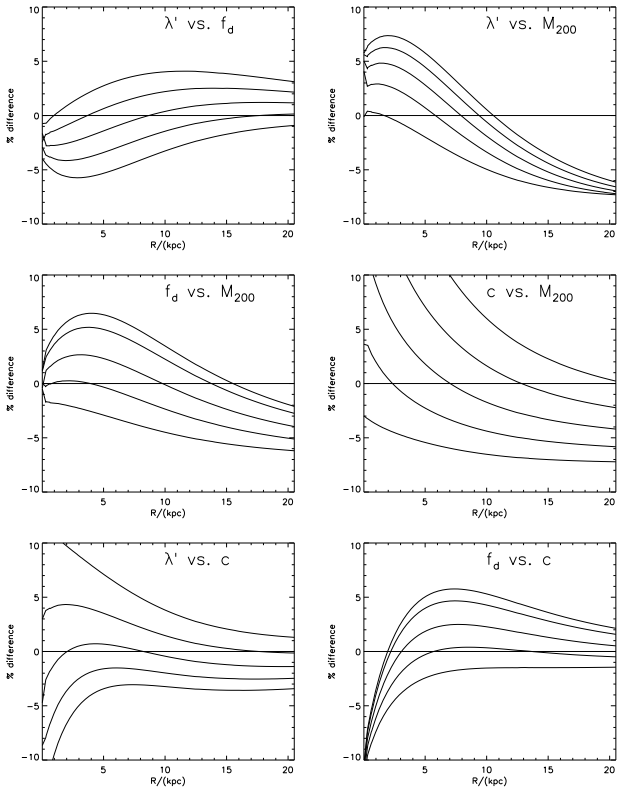

Figure 12. The percentage difference between two rotation curves for which two parameters are changed at the time while the other two are kept constant in a fiducial model with (M_{200}, λ', f_d, c)=(1×10^{11}, 0.05, 0.01, 10). The different curves correspond to variations of 5, 10, 15, 20 and 25% in the model parameters. The two parameters that are changed are shown on the top of each panel. The fiducial model is shown as a solid horizontal line. If the rotation curve is known with less accuracy than the typical variation among parameters, these will be degenerated.

than 5%, then there are clear degeneracies in the $\lambda' - f_d$, $\lambda' - M_{200}$ and $f_d - M_{200}$ planes. On the other hand, in the other planes there are no degeneracies if the rotation curve is well-constrained below 2 disk scale-lengths. Therefore, if the rotation curve is known to better than 5%, with significant spatial coverage, degeneracies among the parameters should not arise. Of the various parameter combinations, the most degenerate pair is $\lambda' - f_d$.

We now turn our attention to the actual data. We first choose a good example to illustrate how well degeneracies can be broken. We choose galaxy 11846 from the Courteau (1997) sample. Fig. 13 shows the 95.4% confidence contour for two parameters having been marginalized, i.e. integrated the likelihood ($\mathcal{L} = \exp[-\chi^2/2]$), on the remaining parameters (note that these quoted confidence intervals should not be over-interpreted: the true (larger) uncertainty is likely to be dominated by systematic errors and inadequacies in the model). The confidence contours are indeed rather small, implying errors in the recovered parameters of only about 20%. From a Fisher matrix analysis (see section 5.1) we find that about 20% of the rotation curves in our sample have the above quality, 60% have $\sim 50\%$ errors in the recovered parameters. Only 20% have much larger error bars, with much poorer constraints on the recovered parameters; one of these galaxies is f583-4.

The case of f583-4 is extremely useful to illustrate the large degeneracies that arise due to the lack of spatial resolution in the rotation curve. This has only 9 points with large error bars. Fig. 14 shows the 68.5% confidence contours. These are large and broad, and the parameters are very poorly constrained. This should not come as a surprise since one can hardly expect to constrain well 4 parameters with only 9 points in view of the results from fig. 12. We stress here that 80% of the galaxies in the sample have much better resolution rotation curves thus the recovered parameters are much better constrained.

We explore the dependence of parameters on the spatial resolution of the rotation curve by investigating in further detail e376g2 from the Palunas & Williams (2000) sample. We perform the following manipulations to e376g2: first we have removed all points beyond 10 kpc (no-flat), to produce a rotation curve without the flat part. Next, to the original rotation curve we remove the inner points below a radius of 3 kpc, so there is no rising part of the rotation curve (no-r).

We also select a random subsample, only 1/3 of the original points, from the rotation curve, thus degrading spatial resolution (low-res). Finally, we fit independently the

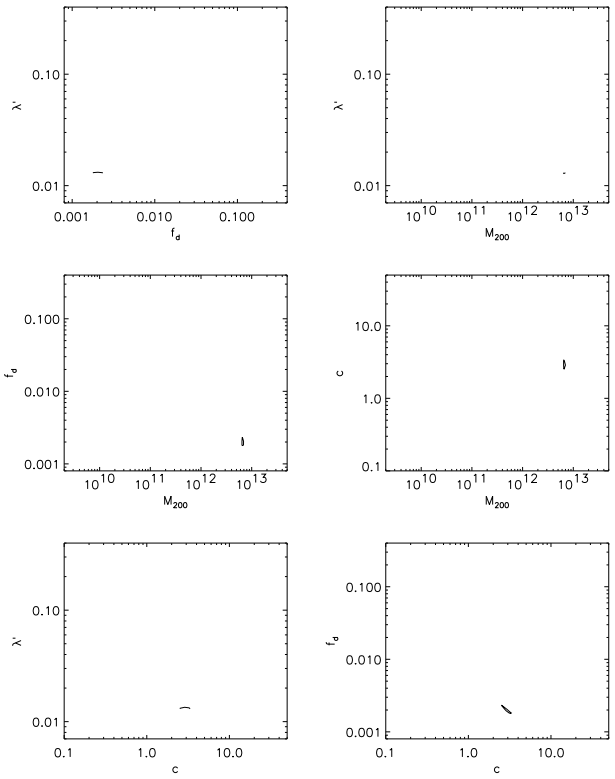

Figure 13. The 95.4% confidence contours for galaxy 11846 in the Courteau sample for a pair of parameters marginalizing over the other two. Note the small size of the confidence regions due to the good spatial sampling of the rotation curve.

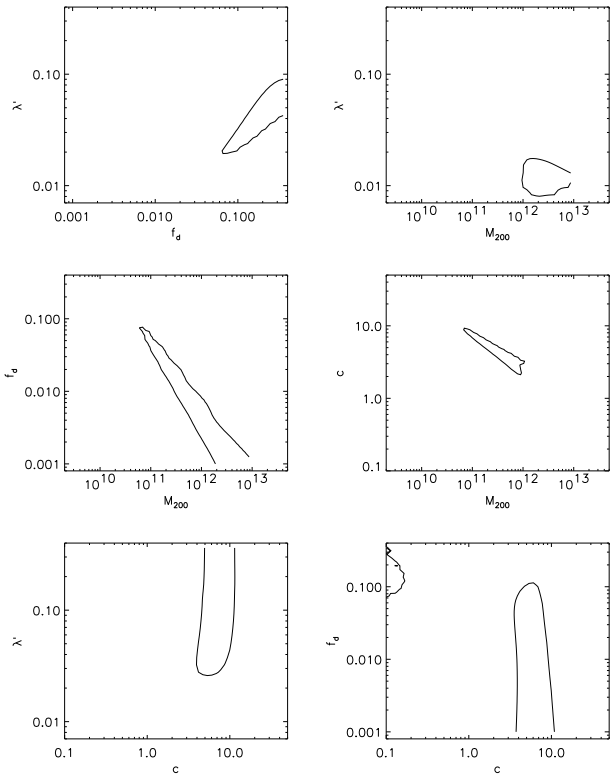

Figure 14. Same as fig. 13 but the galaxy f583-4 from the de Block et al. (2001) sample which has a poor spatially resolved rotation curve. In this case we show the 68.5% confidence contours. Due to the poor spatial resolution the confidence contours are much larger in this case. It is also useful to see that the regions of degeneracy are not inside the avoidance regions.

e376g2	all	no-flat	no-r	low-res	left	right
M_{200}	6 ± 3	5	6	4	10	7
c	4 ± 1	3	4	4	4	2
$f_d \times 10^{-3}$	4 ± 1	6	4	8	2	8
$\lambda' \times 10^{-2}$	13 ± 5	13	13	15	12	13

Table 1. Values of recovered parameters from the rotation curve of e376g2 after having performed several manipulations to its rotation curve (see text). The mass in units of 10^{12} $M_\odot$.

approaching and receding parts of the rotation curve. This gives us a handle on the effect of asymmetries in the rotation curve. The values for the parameters are shown in table 1. Also shown are the values for the full fit (all) with errors obtained from marginalizing over the other three parameters. The variation in the recovered values of λ' is very small, while variations of up to 100% occur for the other parameters. The larger error in the recovered values happens for the low-res case, i.e. when the spatial resolution of the rotation curve is decreased. It is interesting to see how the different parameters are affected. The largest error for M_{200} is for the low-res case, while the largest error for c occurs when only one part of the rotation curve is used. For f_d the largest deviation occurs in the low-res case.

The three rotation curves used in the above example are shown in fig. 15.

5.1 Fisher matrix analysis

When the galaxy sample is large, it might be inefficient to explore the whole likelihood surface as we have done in this case and maybe more important, it might not be possible in the case of very large datasets. Therefore it is useful to use a fast algorithm to estimate the error and, especially, the possible degeneracies. As an alternative to the exact study presented above, and as an illustration for a method that can be suitable for very large data sets, we apply the Fisher matrix analysis to our data set.

We performed a Fisher matrix analysis of the likelihood function $\mathcal{L}$, where $\chi^2 = -2\ln(\mathcal{L})$. Recall that for M parameters, the marginal error on each of the parameters can be obtained, under the assumption of Gaussian likelihood, from the Fisher information matrix

$$F_{ij} \equiv -\left\langle \frac{\partial^2 \ln \mathcal{L}}{\partial\theta_i \partial\theta_j} \right\rangle \tag{21}$$

where i and j run from 1 to M (in our case $M = 4$) and the angle brackets denotes the averaging over many realizations. The marginal error is then

$$\sigma_i = \sqrt{(F^{-1})_{ii}}. \tag{22}$$

Since our best fit parameters are those that maximize the likelihood, a Taylor expansion of $\ln \mathcal{L}$ around $\boldsymbol{\theta}_0$ gives

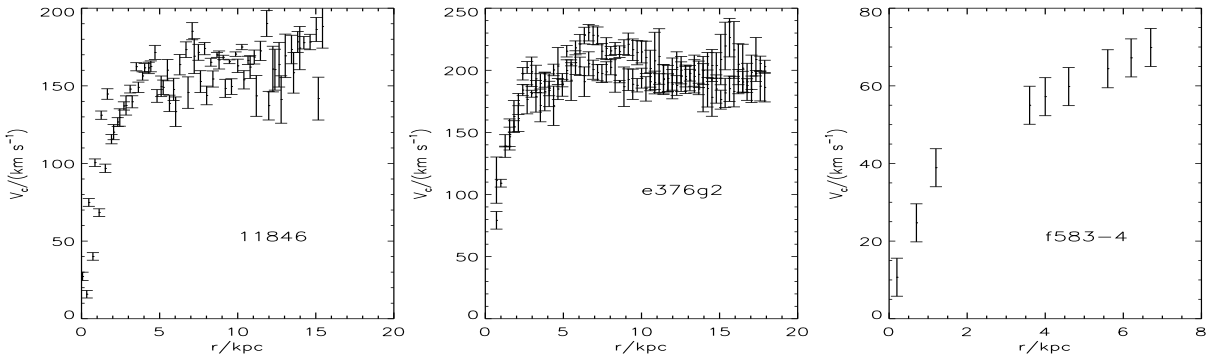

Figure 15. Three examples of rotation curves. The one on the left panel is from the Courteau sample, the one in the middle is from the PW sample and the one on the right panel from the LSB sample.

$$\ln \mathcal{L}(\boldsymbol{\theta}_0 + \Delta\boldsymbol{\theta}) \simeq \ln \mathcal{L}_0 + \frac{1}{2}\frac{\partial^2 \ln \mathcal{L}}{\partial\theta_i\theta_j}\Delta\theta_i\Delta\theta_j. \quad (23)$$

The elements of the Fisher matrix can be estimated as:

$$F_{ii} \simeq - \frac{1}{\Delta\theta_i^2}\left[\ln \mathcal{L}(\boldsymbol{\theta}_0 + \Delta\theta_i\mathbf{e}_i) + \ln \mathcal{L}(\boldsymbol{\theta}_0 - \Delta\theta_i\mathbf{e}_i) - 2\ln \mathcal{L}_0\right]. \quad (24)$$

and

$$\begin{aligned} F_{ij} \simeq \frac{-1}{2\Delta\theta_i\Delta\theta_j} \times & \quad (25) \\ & [\ lnL(\boldsymbol{\theta}_0 + \Delta\theta_i\mathbf{e}_i + \Delta\theta_j\mathbf{e}_j) + \\ & \ln \mathcal{L}(\boldsymbol{\theta}_0 - \Delta\theta_i\mathbf{e}_i - \Delta\theta_j\mathbf{e}_j) - \\ & \ln \mathcal{L}(\boldsymbol{\theta}_0 - \Delta\theta_i\mathbf{e}_i + \Delta\theta_j\mathbf{e}_j) - \\ & \ln \mathcal{L}(\boldsymbol{\theta}_0 + \Delta\theta_i\mathbf{e}_i - \Delta\theta_j\mathbf{e}_j)\ ]. \end{aligned}$$

Furthermore, since the Fisher matrix is symmetric it can be diagonalized ($F = U\Lambda U^T$, where Λ is a diagonal matrix with elements the eigenvectors $\lambda_1, ..., \lambda_M$) and a new orthogonal set of variables built such that $N = U^T O$, where O is the original set of variables (λ, c, f_d and M_{200} in our case). Thus each row of U^T gives the amount by which the original variables are mixed and therefore how degeneracies arise among them.

We have performed the above Fisher analysis on the 400 rotation curves, both for the NFW and the pseudo-isothermal profile. Our conclusions regarding degeneracies are in agreement with the findings of the full analysis performed on galaxies 11846 and f583-4 and illustrated in figures 13 and 14.